

Calculation of the \mathbf{T} matrix in the null-field method with discrete sources

Adrian Doicu and Thomas Wriedt

Institut für Werkstofftechnik, Badgasteiner Strasse 3, 28359 Bremen, Germany

Received February 2, 1999; accepted May 24, 1999; revised manuscript received June 2, 1999

The problem of computing the transition matrix (\mathbf{T} matrix) in the framework of the null-field method with discrete sources is treated. Numerical experiments are performed to investigate the symmetry property of the \mathbf{T} matrix when localized and distributed vector spherical functions are used for solution construction. © 1999 Optical Society of America [S0740-3232(99)01810-4]
OCIS codes: 290.0290, 290.5850.

1. INTRODUCTION

One of the fastest and most powerful numerical tools for computing light scattering by nonspherical particles with use of localized vector spherical functions is the null-field method (otherwise known as the extended boundary-condition method, the Schelkunoff equivalent-current method, the Eswald–Oseen extinction theorem, and the \mathbf{T} -matrix method).^{1–3} A crucial advantage of the null-field method consists in the fact that the transition matrix, or the \mathbf{T} matrix relating the scattered and the incident field coefficients, can be computed easily. The \mathbf{T} matrix is independent of the incident and scattered fields and depends only on the shape, size parameters, and refractive index of the scattering particle as well as on the particle's orientation with respect to the coordinate system. Consequently, the \mathbf{T} matrix need be computed only once and then can be used in computations for any direction of light incidence and scattering. Taking into account the general properties of the \mathbf{T} matrix, on the one hand, Mishchenko has elaborated an efficient analytical method for computing orientationally averaged light-scattering characteristics for ensembles of nonspherical particles.⁴ On the other hand, the \mathbf{T} matrix for a single scatterer can be used successfully for solving a large class of boundary-value problems in electromagnetic scattering theory. In this context, we mention the analysis of multiple-scattering problems^{5,6} and simulation of light scattering by layered or composite objects,^{7–9} and by particles deposited on a surface.¹⁰

However, for particles with extreme geometries or particles with appreciable concavities, the single-spherical-coordinate-based null-field method fails to converge. A number of modifications to the conventional null-field method have been suggested to improve the numerical stability. These techniques include formal modifications of the single-spherical-coordinate-based null-field method,^{11–13} different choices of basis functions,^{14,15} and the application of the spheroidal-coordinate formalism.¹⁶ One of these formal modifications is the null-field method with discrete sources.^{17,18} Essentially, this method entails the use of a number of elementary sources for approximating the surface-current densities. The discrete

sources are placed on a certain support in an additional region with respect to the region where the solution is required. Unknown discrete-source amplitudes that produce the surface densities are computed by use of the null-field condition of the total electric field inside the particle surface.

The aim of our contribution is to compute the transition matrix in the framework of the null-field method with discrete sources. We intend to show the superior efficiency of this method over the conventional approach, especially for analyzing particles with extreme geometries.

2. MATHEMATICAL FORMULATION

Let us consider a three-dimensional space D consisting of the union of a closed surface S , its interior D_i , and its exterior D_s . We denote by k_t the wave number in the domain D_t , where $k_t = k\sqrt{\varepsilon_t\mu_t}$ and $k = \omega/c$; ε_t and μ_t stand for the relative electric permittivity and relative magnetic permeability, respectively, of the domain D_t ; ω is the frequency; c is the speed of wave propagation for the electromagnetic field in free space; and $t = s, i$.

The transmission boundary-value problem can be formulated as follows. Let $\mathbf{E}_0, \mathbf{H}_0$ be an entire solution to the Maxwell equations representing an incident electromagnetic field. Find the vector fields, $\mathbf{E}_s, \mathbf{H}_s \in C^1(D_s) \cap C(\bar{D}_s)$ and $\mathbf{E}_i, \mathbf{H}_i \in C^1(D_i) \cap C(\bar{D}_i)$ that satisfy the Maxwell equations

$$\begin{aligned}\nabla \times \mathbf{E}_t &= jk\mu_t\mathbf{H}_t, \\ \nabla \times \mathbf{H}_t &= -jk\varepsilon_t\mathbf{E}_t,\end{aligned}\quad (1)$$

in D_t , where $t = s, i$, and two transmission conditions,

$$\begin{aligned}\mathbf{n} \times \mathbf{E}_i - \mathbf{n} \times \mathbf{E}_s &= \mathbf{n} \times \mathbf{E}_0, \\ \mathbf{n} \times \mathbf{H}_i - \mathbf{n} \times \mathbf{H}_s &= \mathbf{n} \times \mathbf{H}_0,\end{aligned}\quad (2)$$

on S . In addition, the scattered field $\mathbf{E}_s, \mathbf{H}_s$ must satisfy the Silver–Müller radiation condition uniformly for all directions \mathbf{x}/x . It is known that the transmission boundary-value problem possesses a unique solution.¹⁹

For solving the transmission boundary-value problem in the framework of the null-field method with discrete

sources, the scattering object is replaced by a set of surface-current densities \mathbf{e} and \mathbf{h} , so that in the exterior domain the sources and fields are exactly the same as those that exist in the original scattering problem. The entire analysis can conveniently be broken down into three steps.

In the first step, a set of integral equations for the surface-current densities \mathbf{e} and \mathbf{h} is derived for a variety of discrete sources. Physically, the set of integral equations in question guarantees the null-field condition within D_i . It is noted that localized and distributed vector spherical functions, magnetic and electric dipoles, or vector Mie potentials can be used as discrete sources. Essentially, the null-field method with discrete sources consists of the projection relations,

$$\int_S [(\mathbf{e} - \mathbf{e}_0) \cdot \Psi_\nu^3 + j\sqrt{\frac{\mu_s}{\epsilon_s}}(\mathbf{h} - \mathbf{h}_0) \cdot \Phi_\nu^3] dS = 0$$

$$\int_S [(\mathbf{e} - \mathbf{e}_0) \cdot \Phi_\nu^3 + j\sqrt{\frac{\mu_s}{\epsilon_s}}(\mathbf{h} - \mathbf{h}_0) \cdot \Psi_\nu^3] dS = 0,$$

$\nu = 1, 2, \dots, \quad (3)$

where $\mathbf{e}_0 = \mathbf{n} \times \mathbf{E}_0$ and $\mathbf{h}_0 = \mathbf{n} \times \mathbf{H}_0$ are the tangential components of the incident electric and magnetic fields. The set $\{\Psi_\nu^3, \Phi_\nu^3\}_{\nu=1,2,\dots}$ consists of radiating solutions to Maxwell's equations and depends on the system of discrete sources that is used for imposing the null-field condition. Actually, this set together with the set of regular solutions to Maxwell's equations $\{\Psi_\nu^1, \Phi_\nu^1\}_{\nu=1,2,\dots}$ stands for

• localized vector spherical functions $\{\mathbf{M}_{mn}^{1,3}, \mathbf{N}_{mn}^{1,3}\}_{m \in \mathbf{Z}, n \geq \max(1, |m|)}$,

$$\mathbf{M}_{mn}^{1,3}(k\mathbf{x}) = \sqrt{D_{mn}} z_n(kr) \times \left[jm \frac{P_n^m(\cos \theta)}{\sin \theta} \mathbf{e}_\theta - \frac{dP_n^m(\cos \theta)}{d\theta} \mathbf{e}_\phi \right] \exp(jm\phi)$$

$$\mathbf{N}_{mn}^{1,3}(k\mathbf{x}) = \sqrt{D_{mn}} \left\{ n(n+1) \times \frac{z_n(kr)}{kr} P_n^m(\cos \theta) \exp(jm\phi) \mathbf{e}_r + \frac{[krz_n(kr)]'}{kr} \left[\frac{dP_n^m(\cos \theta)}{d\theta} \mathbf{e}_\theta + jm \frac{P_n^m(\cos \theta)}{\sin \theta} \mathbf{e}_\phi \right] \right\} \exp(jm\phi),$$

where $(\mathbf{e}_r, \mathbf{e}_\theta, \mathbf{e}_\phi)$ are the unit vectors in spherical coordinates, z_n designates the spherical Bessel functions j_n or the spherical Hankel functions of the first kind h_n^1 , P_n^m denotes the associated Legendre polynomial of order n and m , and D_{mn} is a normalization constant given by

$$D_{mn} = \frac{2n+1}{4n(n+1)} \cdot \frac{(n-|m|)!}{(n+|m|)!};$$

• distributed vector spherical functions $\{\mathcal{M}_{mn}^{1,3}, \mathcal{N}_{mn}^{1,3}\}_{m \in \mathbf{Z}, n=1,2,\dots}$,

$$\mathcal{M}_{mn}^{1,3}(k\mathbf{x}) = \mathbf{M}_{m,|m|+l}^{1,3}[k(\mathbf{x} - z_n \mathbf{e}_3)],$$

$$\mathbf{x} \in \mathbf{R}^3 - \{z_n \mathbf{e}_3\}_{n=1}^\infty,$$

$$\mathcal{N}_{mn}^{1,3}(k\mathbf{x}) = \mathbf{N}_{m,|m|+l}^{1,3}[k(\mathbf{x} - z_n \mathbf{e}_3)],$$

$$\mathbf{x} \in \mathbf{R}^3 - \{z_n \mathbf{e}_3\}_{n=1}^\infty,$$

where $m \in \mathbf{Z}$, $n = 1, 2, \dots$, $l = 1$ if $m = 0$ and $l = 0$ if $m \neq 0$, and $\{z_n\}_{n=1}^\infty$ is a set of points located on a segment Γ_z of the z axis;

• magnetic and electric dipoles $\{\mathcal{M}_{ni}^{1,3}, \mathcal{N}_{ni}^{1,3}\}_{n=1,2,\dots, i=1,2}$,

$$\mathcal{M}_{ni}^{1,3}(k\mathbf{x}) = \mathbf{m}(\mathbf{x}_n^\pm, \mathbf{x}, \tau_{ni}^\pm), \quad \mathbf{x} \in \mathbf{R}^3 - \{\mathbf{x}_n^\pm\}_{n=1}^\infty,$$

$$\mathcal{N}_{ni}^{1,3}(k\mathbf{x}) = \mathbf{n}(\mathbf{x}_n^\pm, \mathbf{x}, \tau_{ni}^\pm), \quad \mathbf{x} \in \mathbf{R}^3 - \{\mathbf{x}_n^\pm\}_{n=1}^\infty,$$

where $n = 1, 2, \dots$, $i = 1, 2$, τ_{n1} and τ_{n2} are two tangential linear independent unit vectors at the point \mathbf{x}_n ;

$$\mathbf{m}(\mathbf{x}, \mathbf{y}, \mathbf{a}) = \frac{1}{k^2} \mathbf{a}(\mathbf{x}) \times \nabla_y g(\mathbf{x}, \mathbf{y}, k),$$

$$\mathbf{n}(\mathbf{x}, \mathbf{y}, \mathbf{a}) = \frac{1}{k} \nabla_y \times \mathbf{m}(\mathbf{x}, \mathbf{y}, \mathbf{a}), \quad \mathbf{x} \neq \mathbf{y},$$

where the sequence $\{\mathbf{x}_n^-\}_{n=1}^\infty$ is dense on a smooth surface S^- enclosed in D_i and the sequence $\{\mathbf{x}_n^+\}_{n=1}^\infty$ is dense on a smooth surface S^+ enclosing D_i ; or, finally, for the set of

• vector Mie potentials $\{\mathcal{M}_n^{1,3}, \mathcal{N}_n^{1,3}\}_{n=1,2,\dots}$,

$$\mathcal{M}_n^{1,3}(k\mathbf{x}) = \frac{1}{k} \nabla \times [\phi_n^\pm(\mathbf{x}) \mathbf{x}], \quad \mathbf{x} \in \mathbf{R}^3 - \{\mathbf{x}_n^\pm\}_{n=1}^\infty,$$

$$\mathcal{N}_n^{1,3}(k\mathbf{x}) = \frac{1}{k} \nabla \times \mathcal{M}_n^{1,3}(k\mathbf{x}), \quad \mathbf{x} \in \mathbf{R}^3 - \{\mathbf{x}_n^\pm\}_{n=1}^\infty,$$

where the Green functions

$$\phi_n^\pm(\mathbf{x}) = g(\mathbf{x}_n^\pm, \mathbf{x}, k), \quad n = 1, 2, \dots,$$

have singularities $\{\mathbf{x}_n^-\}_{n=1}^\infty$ and $\{\mathbf{x}_n^+\}_{n=1}^\infty$ distributed on the auxiliary surfaces S^- and S^+ , respectively. By convention, when we refer to null-field equations (3) we refer implicitly to all equivalent forms of these equations.

In the second step, the surface current densities are approximated by fields of discrete sources. In this context let \mathbf{e} and \mathbf{h} solve null-field equations (3) and assume that the system $\{\mathbf{n} \times \Psi_\mu^1, \mathbf{n} \times \Phi_\mu^1\}_{\mu=1}^\infty$ forms a Schauder basis in $\mathcal{L}_{\tan}^2(S)$. Then there exists a sequence $\{a_\mu, b_\mu\}_{\mu=1}^\infty$ such that

$$\mathbf{e}(\mathbf{y}) = \sum_{\mu=1}^\infty a_\mu \mathbf{n} \times \Psi_\mu^1(k_i \mathbf{y}) + b_\mu \mathbf{n} \times \Phi_\mu^1(k_i \mathbf{y}), \quad \mathbf{y} \in S,$$

$$\mathbf{h}(\mathbf{y}) = -j \sqrt{\frac{\epsilon_i}{\mu_i}} \sum_{\mu=1}^\infty a_\mu \mathbf{n} \times \Phi_\mu^1(k_i \mathbf{y}) + b_\mu \mathbf{n} \times \Psi_\mu^1(k_i \mathbf{y}),$$

$\mathbf{y} \in S. \quad (4)$

We recall that a system $\{\psi_i\}_{i=1}^\infty$ is called a Schauder basis of a Banach space X if any element $u \in X$ can be uniquely represented as $u = \sum_{i=1}^\infty \alpha_i \psi_i$, where the convergence of

the series is in the norm of X . It is noted that in the case of localized vector spherical functions the notion of Schauder basis is closely connected to the Rayleigh hypothesis. This hypothesis says that the series representation of the scattered field in terms of radiating localized vector spherical functions, which uniformly converges outside the circumscribing sphere, also converges on S .

In the third step, once the surface current densities are determined, the scattered field outside the circumscribing sphere is obtained by use of the representation theorem. We get the series representation

$$\mathbf{E}_s(\mathbf{x}) = \sum_{\nu=1}^{\infty} f_{\nu} \mathbf{M}_{\nu}^3(k_s \mathbf{x}) + g_{\nu} \mathbf{N}_{\nu}^3(k_s \mathbf{x}), \quad (5)$$

where

$$\begin{aligned} f_{\nu} &= \frac{jk_s^2}{\pi} \int_S \left[\mathbf{e}(\mathbf{y}) \cdot \mathbf{N}_{\nu}^1(k_s \mathbf{y}) \right. \\ &\quad \left. + j \sqrt{\frac{\mu_s}{\epsilon_s}} \mathbf{h}(\mathbf{y}) \cdot \mathbf{M}_{\nu}^1(k_s \mathbf{y}) \right] dS(\mathbf{y}) \\ g_{\nu} &= \frac{jk_s^2}{\pi} \int_S \left[\mathbf{e}(\mathbf{y}) \cdot \mathbf{M}_{\nu}^1(k_s \mathbf{y}) \right. \\ &\quad \left. + j \sqrt{\frac{\mu_s}{\epsilon_s}} \mathbf{h}(\mathbf{y}) \cdot \mathbf{N}_{\nu}^1(k_s \mathbf{y}) \right] dS(\mathbf{y}). \end{aligned} \quad (6)$$

Here, $\bar{\nu}$ is a complex index incorporating $-m$ and n ; i.e., $\bar{\nu} = (-m, n)$.

Now, for deriving the \mathbf{T} matrix let us assume that the incident field can be expressed inside a finite region containing S as a series of regular vector spherical functions:

$$\begin{aligned} \mathbf{E}_0(\mathbf{x}) &= \sum_{\nu=1}^{\infty} a_{\nu}^0 \mathbf{M}_{\nu}^1(k_s \mathbf{x}) + b_{\nu}^0 \mathbf{N}_{\nu}^1(k_s \mathbf{x}), \\ \mathbf{H}_0(\mathbf{x}) &= -j \sqrt{\frac{\epsilon_s}{\mu_s}} \sum_{\nu=1}^{\infty} a_{\nu}^0 \mathbf{N}_{\nu}^1(k_s \mathbf{x}) + b_{\nu}^0 \mathbf{M}_{\nu}^1(k_s \mathbf{x}). \end{aligned} \quad (7)$$

Then, using Eqs. (3)–(7), we see that the relation between the scattered and the incident field coefficients is linear and is given by a transition matrix \mathbf{T} as follows:

$$\begin{bmatrix} f_{\nu} \\ g_{\nu} \end{bmatrix} = \mathbf{T} \begin{bmatrix} a_{\nu}^0 \\ b_{\nu}^0 \end{bmatrix}. \quad (8)$$

Here

$$\mathbf{T} = \mathbf{B} \mathbf{A}^{-1} \mathbf{A}_0, \quad (9)$$

where \mathbf{A} , \mathbf{B} , and \mathbf{A}_0 are block matrices written in general as

$$\mathbf{X} = \begin{bmatrix} X_{\nu\mu}^{11} & X_{\nu\mu}^{12} \\ X_{\nu\mu}^{21} & X_{\nu\mu}^{22} \end{bmatrix}, \quad \nu, \mu = 1, 2, \dots,$$

with \mathbf{X} standing for \mathbf{A} , \mathbf{B} , and \mathbf{A}_0 . Explicit expressions for the elements of these matrices are given in Appendix A.

It is noted that the exact infinite \mathbf{T} matrix is independent of the expansion systems used on S . However, the approximate truncated matrix, computed according to

$$\mathbf{T}_N = \mathbf{B}_N \mathbf{A}_N^{-1} \mathbf{A}_{0N}, \quad (10)$$

does contain such a dependence.

The transition matrix has some unitarity and symmetry properties. These properties can be established, for example, by consideration of the energy flow through a finite sphere and the reciprocity relations.²⁰ The general symmetry relations for the \mathbf{T} -matrix elements read as

$$T_{-mn-m'n'}^{ij} = T_{m'n'mn}^{ji}. \quad (11)$$

For an axisymmetric particle, the \mathbf{T} matrix becomes diagonal with respect to the azimuthal indices m and m' , and we have

$$\begin{aligned} T_{mnm'n'}^{ij} &= \delta_{mm'} T_{mnm'n'}^{ij}, \\ T_{mnmn'}^{ij} &= (-1)^{i+j} T_{-mn-mn'}^{ij}. \end{aligned} \quad (12)$$

In this case the symmetry relation takes the form

$$T_{mnmn'}^{ij} = (-1)^{i+j} T_{mn'mn}^{ji}. \quad (13)$$

In general, in the null-field approach the dependence of the numerical results on the truncation order is the main feature that can be taken as a basis for statements concerning the accuracy of the results. In addition, one can check general features such as the symmetry and unitarity of the transition matrix. Actually, the symmetry errors give a rough idea concerning the convergence to be expected in the computations of the solution, but the details are hard to predict.

3. NUMERICAL SIMULATIONS

In this section we present some computer simulations for analyzing the symmetry of the transition matrix. For our numerical experiments we use localized and distributed vector spherical functions. The use of lowest-order vector spherical functions is most effective for axisymmetric particles. By using a system of vector spherical functions distributed along the axis of revolution, it is possible to reduce the problem of the approximation of surface-current densities to a sequence of one-dimensional problems relative to the Fourier harmonics of the surface currents. The position of the poles where the null-field condition is imposed should be correlated with the singularities of analytic continuation of the scattered field inside D_i . In this context, locating the poles on the axis of revolution does not offer sufficiently large flexibility for analyzing various particle geometries. In the case of prolate scatterers, for example, the choice of multipoles on the symmetry axis adequately describes the particle geometry, but this arrangement is not suitable for oblate scatterers. To master this problem, we use the analytic continuation of the solution into the complex plane along the source coordinate z_n .¹⁷ Actually, the poles are positioned in the connected domain whose boundary coincides with the image of the surface generatrix in the complex plane. It is noted that in the case of localized vector spherical functions, the matrix \mathbf{A}_0 is a diagonal matrix. This case corresponds to the conventional null-field method given by Waterman.¹

In our first example we consider the scattering by prolate spheroids with large semiaxis $k_s a = 10$ and small semiaxis varying between $k_s b = 0.5$ and $k_s b = 5$. The refractive index is $M = 1.5$. The incident field is a plane wave traveling along the z axis, which corresponds to the

particle symmetry axis. In the case of distributed vector spherical functions, the poles are located at the segment $\Gamma_z = [-0.9a, 0.9a]$ of the z axis. In Fig. 1 we present the relative symmetry error of the transition matrix,

$$\sigma_m = \sum_{i=1}^2 \sum_{n=1}^N \sum_{n'>n}^N |T_{mnmn'}^{ii} - T_{mn'mn}^{ii}| / |T_{mnmn'}^{ii}| + \sum_{n,n'=1}^N |T_{mnmn'}^{12} + T_{mn'mn}^{21}| / |T_{mnmn'}^{12}| \quad [\%], \quad (14)$$

for the azimuthal mode $m = 1$. The plotted data show that the symmetry of the transition matrix computed with localized vector spherical functions deteriorates significantly when the aspect ratio increases—that is, for $a/b < 5$. In contrast, the distributed vector spherical functions lead to a transition matrix with high symmetry even for an aspect ratio of $a/b = 20$. The curves also demonstrate that the relative symmetry error is in general lower for distributed sources. In Fig. 2 we plot the relative matrix error defined as

$$\epsilon_m = \sum_{i,j=1}^2 \sum_{n,n'=1}^N (T_{mnmn'}^{ij,A} - T_{mnmn'}^{ij,B}) / T_{mnmn'}^{ij,A} \quad [\%]. \quad (15)$$

The superscripts A and B correspond to the null-field method with distributed and localized vector spherical functions, respectively. Clearly, the transition matrix computed by the conventional method deviates significantly from that obtained by the null-field method with distributed sources when $a/b < 5$. In fact, below this limit the conventional method does not converge. This is demonstrated in Fig. 3 for a spheroid with $k_s a = 10$ and $k_s b = 1$. Here we plot the normalized differential scattering cross section at a scattering angle of 180° as a function of truncation index N .

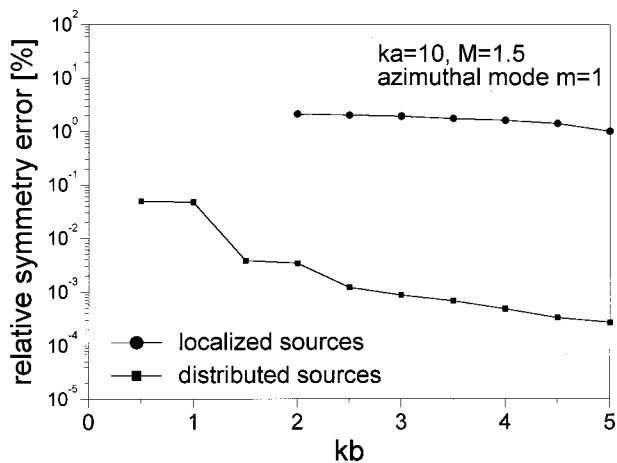


Fig. 1. Relative symmetry error of the transition matrix for the azimuthal mode $m = 1$ for prolate spheroids with large semi-axis $k_s a = 10$ and small semi-axis varying between $k_s b = 0.5$ and $k_s b = 5$. The refractive index of the particle is $M = 1.5$. The incident field is a p -polarized plane wave traveling along the z axis, which corresponds to the particle symmetry axis. The truncation index is $N = 17$ for all cases.

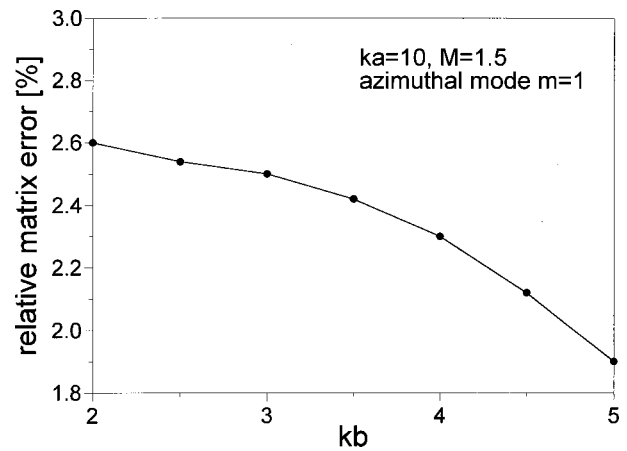


Fig. 2. Relative error between the transition matrices computed by the null-field method with localized and distributed vector spherical functions and by the conventional method for prolate spheroids with large semi-axis $k_s a = 10$ and small semi-axis varying between $k_s b = 2$ and $k_s b = 5$. The refractive index of the particle is $M = 1.5$, and the truncation index is $N = 17$.

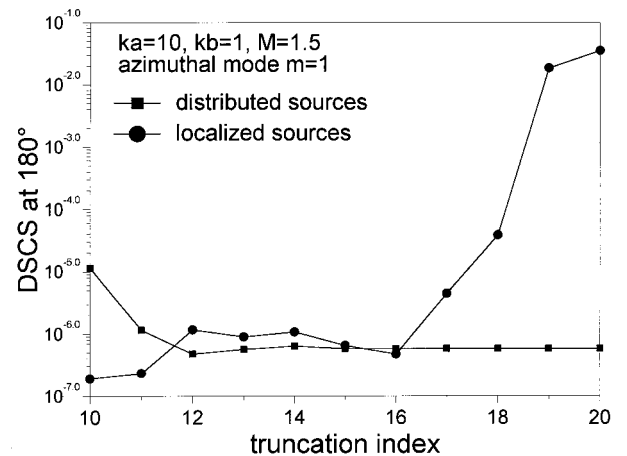


Fig. 3. Normalized differential scattering cross section at a scattering angle of 180° versus truncation index. The particle is a prolate spheroid with $k_s a = 10$, $k_s b = 1$, and $M = 1.5$. The incident field is a p -polarized plane wave traveling along the z axis, which corresponds to the particle symmetry axis. The curves correspond to the azimuthal mode $m = 1$.

In Fig. 4 we consider an oblate spheroid with large semi-axis $k_s b = 10$ and small semi-axis varying as before between $k_s a = 1$ and $k_s a = 5$. The refractive index is $M = 1.5$. In this case the poles of the distributed vector spherical functions are located in the complex plane along the imaginary axis. The same alteration of the matrix symmetry is observed in the case of localized vector spherical functions when semi-axis a decreases. The symmetry is destroyed for $k_s a < 3$. In contrast, when distributed sources are used, the relative symmetry error is small; for example, in the case $k_s a = 1$ it was found that $\epsilon_1 < 0.7\%$. The relative matrix error plotted in Fig. 5 also indicates that the conventional method gives erroneous results for $k_s a < 3$.

When localized sources are used as basis and testing functions, the symmetry of the transition matrix begins to deteriorate as the refractive index increases. This is illustrated in Fig. 6 for a prolate spheroid with $k_s a = 10$

and $k_s b = 2$. The refractive index M increases from 1.5 to 4. The plotted data show that the null-field method with distributed sources has a relative symmetry error smaller than 0.2%. In contrast, the relative symmetry error of the null-field method with localized sources is larger than 40% when $M > 2$. Consequently, instability and convergence problems are associated with the single-spherical-coordinate-based null-field method as M increases. To show the oscillating behavior of the solution, in Fig. 7 we have plotted the normalized differential scattering cross section at a scattering angle of 180° as a function of truncation index N . The data correspond to a refractive index $M = 4$.

We conclude this section by mentioning that the null-field method with distributed sources needs computations that are longer than those in the conventional approach. For instance, for a prolate spheroid with $k_s a = 10$, $k_s b$

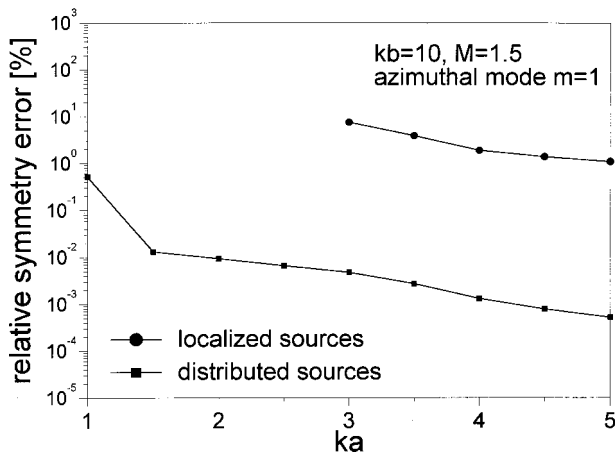


Fig. 4. Relative symmetry error of the transition matrix for the azimuthal mode $m = 1$ for an oblate spheroid with large semiaxis $k_s b = 10$ and small semiaxis varying between $k_s a = 1$ and $k_s a = 5$. The refractive index of the particle is $M = 1.5$. The incident field is a p -polarized plane wave traveling along the z axis, which corresponds to the particle symmetry axis. The truncation index is $N = 17$ for all cases.

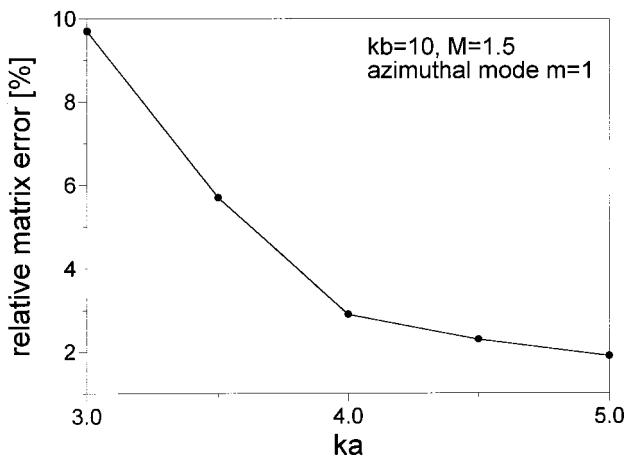


Fig. 5. Relative error between the transition matrices computed by the null-field method with localized and distributed vector spherical functions for oblate spheroids with large semiaxis $k_s b = 10$ and small semiaxis varying between $k_s a = 3$ and $k_s a = 5$. The refractive index of the particle is $M = 1.5$, and the truncation index is $N = 17$.

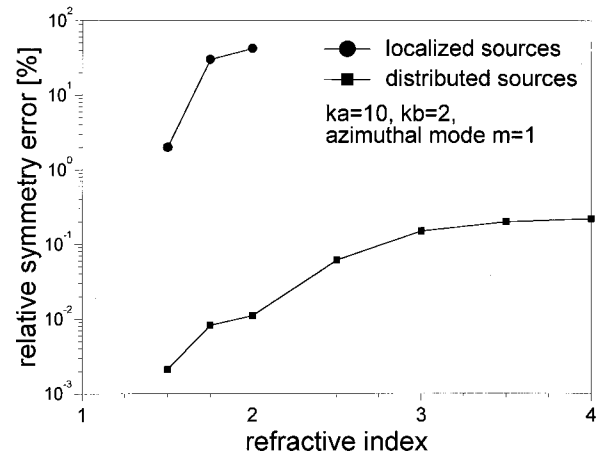


Fig. 6. Relative symmetry error of the transition matrix for the azimuthal mode $m = 1$ for a prolate spheroid with $k_s a = 10$ and $k_s b = 2$ when the refractive index varies from $M = 1.5$ to $M = 4$. The incident field is a p -polarized plane wave traveling along the z axis, which corresponds to the particle symmetry axis. The values of the truncation index are $N = 17, 18, 20, 24, 26, 28,$ and 30 and correspond to values of the refractive index $M = 1.5, 1.75, 2.0, 2.5, 3.0, 3.5,$ and 4.0 , respectively.

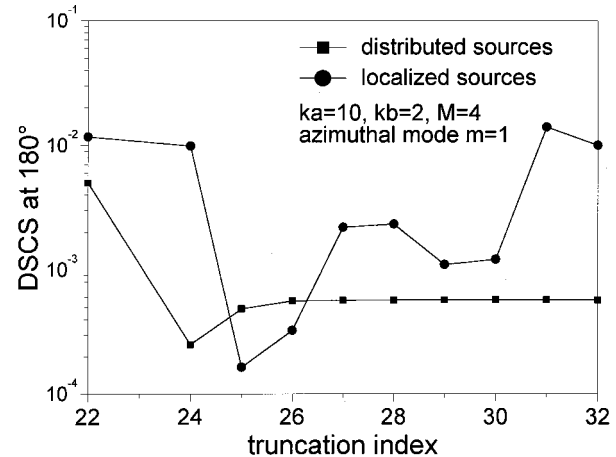


Fig. 7. Normalized differential scattering cross section at a scattering angle of 180° versus truncation index for a prolate spheroid with $k_s a = 10$, $k_s b = 2$, and $M = 4$. The incident field is a p -polarized plane wave traveling along the z axis, which corresponds to the particle symmetry axis. The curves correspond to the azimuthal mode $m = 1$.

$= 2$, and $M = 1.5$, we find that the CPU time of the null-field method with distributed vector spherical functions is 0.335 s, whereas the CPU time of the null-field method with localized vector spherical functions is 0.183 s. The calculations were performed on an IBM workstation RS/6000.

4. CONCLUSIONS

An efficient way for computing the transition matrix in the framework of the null-field method with discrete sources is presented. Numerical experiments were performed for prolate and oblate spheroids with gradually deformed shape and by varying the refractive index. The results indicate that the transition matrix computed in the framework of the null-field method with distributed

vector spherical functions has a high symmetry even for particles with extreme geometries and high values of the refractive index. In contrast, the symmetry of the transition matrix computed by the conventional approach (with localized vector spherical functions) is altered, and the algorithm fails to converge. This is an additional argument that the null-field method with discrete sources can be used in the mathematical modeling of difficult scattering problems.

APPENDIX A

The block elements of matrices **A**, **B**, and **A**₀ are given by

$$\begin{aligned}
 A_{\nu\mu}^{11} &= \int_S [(\mathbf{n} \times \boldsymbol{\Psi}_\mu^1) \cdot \boldsymbol{\Psi}_\nu^3 + M(\mathbf{n} \times \boldsymbol{\Phi}_\mu^1) \cdot \boldsymbol{\Phi}_\nu^3] dS, \\
 A_{\nu\mu}^{12} &= \int_S [(\mathbf{n} \times \boldsymbol{\Phi}_\mu^1) \cdot \boldsymbol{\Psi}_\nu^3 + M(\mathbf{n} \times \boldsymbol{\Psi}_\mu^1) \cdot \boldsymbol{\Phi}_\nu^3] dS, \\
 A_{\nu\mu}^{21} &= \int_S [(\mathbf{n} \times \boldsymbol{\Psi}_\mu^1) \cdot \boldsymbol{\Phi}_\nu^3 + M(\mathbf{n} \times \boldsymbol{\Phi}_\mu^1) \cdot \boldsymbol{\Psi}_\nu^3] dS, \\
 A_{\nu\mu}^{22} &= \int_S [(\mathbf{n} \times \boldsymbol{\Phi}_\mu^1) \cdot \boldsymbol{\Phi}_\nu^3 + M(\mathbf{n} \times \boldsymbol{\Psi}_\mu^1) \cdot \boldsymbol{\Psi}_\nu^3] dS, \quad (\text{A1}) \\
 B_{\nu\mu}^{11} &= \frac{jk_s^2}{\pi} \int_S [(\mathbf{n} \times \boldsymbol{\Psi}_\mu^1) \cdot \mathbf{N}_\nu^1 + M(\mathbf{n} \times \boldsymbol{\Phi}_\mu^1) \cdot \mathbf{M}_\nu^1] dS, \\
 B_{\nu\mu}^{12} &= \frac{jk_s^2}{\pi} \int_S [(\mathbf{n} \times \boldsymbol{\Phi}_\mu^1) \cdot \mathbf{N}_\nu^1 + M(\mathbf{n} \times \boldsymbol{\Psi}_\mu^1) \cdot \mathbf{M}_\nu^1] dS, \\
 B_{\nu\mu}^{21} &= \frac{jk_s^2}{\pi} \int_S [(\mathbf{n} \times \boldsymbol{\Psi}_\mu^1) \cdot \mathbf{M}_\nu^1 + M(\mathbf{n} \times \boldsymbol{\Phi}_\mu^1) \cdot \mathbf{N}_\nu^1] dS, \\
 B_{\nu\mu}^{22} &= \frac{jk_s^2}{\pi} \int_S [(\mathbf{n} \times \boldsymbol{\Phi}_\mu^1) \cdot \mathbf{M}_\nu^1 + M(\mathbf{n} \times \boldsymbol{\Psi}_\mu^1) \cdot \mathbf{N}_\nu^1] dS, \quad (\text{A2})
 \end{aligned}$$

and

$$\begin{aligned}
 A_{0\nu\mu}^{11} &= \int_S [(\mathbf{n} \times \mathbf{M}_\mu^1) \cdot \boldsymbol{\Psi}_\nu^3 + (\mathbf{n} \times \mathbf{N}_\mu^1) \cdot \boldsymbol{\Phi}_\nu^3] dS, \\
 A_{0\nu\mu}^{12} &= \int_S [(\mathbf{n} \times \mathbf{N}_\mu^1) \cdot \boldsymbol{\Psi}_\nu^3 + (\mathbf{n} \times \mathbf{M}_\mu^1) \cdot \boldsymbol{\Phi}_\nu^3] dS, \\
 A_{0\nu\mu}^{21} &= \int_S [(\mathbf{n} \times \mathbf{M}_\mu^1) \cdot \boldsymbol{\Phi}_\nu^3 + (\mathbf{n} \times \mathbf{N}_\mu^1) \cdot \boldsymbol{\Psi}_\nu^3] dS, \\
 A_{0\nu\mu}^{22} &= \int_S [(\mathbf{n} \times \mathbf{N}_\mu^1) \cdot \boldsymbol{\Phi}_\nu^3 + (\mathbf{n} \times \mathbf{M}_\mu^1) \cdot \boldsymbol{\Psi}_\nu^3] dS, \quad (\text{A3})
 \end{aligned}$$

respectively. Here, M is the refractive index and is given by $M = \sqrt{\epsilon_i/\epsilon_s}$.

REFERENCES

1. P. C. Waterman, "New formulation of acoustic scattering," *J. Acoust. Soc. Am.* **45**, 1417–1429 (1969).
2. P. C. Waterman, "Symmetry, unitarity and geometry in electromagnetic scattering," *Phys. Rev. D* **3**, 825–839 (1971).
3. P. W. Barber and S. C. Hill, *Light Scattering by Particles: Computational Methods* (World Scientific, Singapore, 1990).
4. M. I. Mishchenko, "Light scattering by randomly oriented axially symmetric particles," *J. Opt. Soc. Am. A* **8**, 871–882 (1991).
5. B. Peterson and S. Ström, "T-matrix for electromagnetic scattering from an arbitrary number of scatterers," *Phys. Rev. D* **8**, 3661–3678 (1973).
6. D. W. Mackowski, "Calculations of total cross sections of multiple-sphere clusters," *J. Opt. Soc. Am. A* **11**, 2851–2861 (1994).
7. D. Ngo, G. Videen, and P. Chylek, "A Fortran code for the scattering of EM waves by a sphere with a nonconcentric spherical inclusion," *Comput. Phys. Commun.* **99**, 94–112 (1996).
8. G. Videen, D. Ngo, P. Chylek, and R. G. Pinnick, "Light scattering from a sphere with an irregular inclusion," *J. Opt. Soc. Am. A* **12**, 922–928 (1995).
9. Wenxin Zheng, "The null-field approach to electromagnetic scattering from composite objects: the case with three or more constituents," *IEEE Trans. Antennas Propag.* **36**, 1396–1400 (1988).
10. T. Wriedt and A. Doicu, "Light scattering from a particle on or near a surface," *Opt. Commun.* **152**, 376–384 (1998).
11. A. Boström, "Scattering of acoustic waves by a layered elastic obstacle immersed in a fluid: an improved null-field approach," *J. Acoust. Soc. Am.* **76**, 588–593 (1984).
12. M. F. Iskander, A. Lakhtakia, and C. H. Durney, "A new procedure for improving the solution stability and extending the frequency range of the EBCM," *IEEE Trans. Antennas Propag.* **AP-31**, 317–324 (1983).
13. M. F. Iskander and A. Lakhtakia, "Extension of the iterative EBCM to calculate scattering by low-loss or lossless elongated dielectric objects," *Appl. Opt.* **23**, 948–953 (1984).
14. R. H. T. Bates and D. J. N. Wall, "Null field approach to scalar diffraction: I. General method; II. Approximate methods; III. Inverse methods," *Philos. Trans. R. Soc. London A* **287**, 45–117 (1977).
15. A. Lakhtakia, M. F. Iskander, and C. H. Durney, "An iterative EBCM for solving the absorption characteristics of lossy dielectric objects of large aspect ratios," *IEEE Trans. Microwave Theory Tech.* **MTT-31**, 640–647 (1983).
16. R. H. Hackman, "The transition matrix for acoustic and elastic wave scattering in prolate spheroidal coordinates," *J. Acoust. Soc. Am.* **75**, 35–45 (1984).
17. A. Doicu and T. Wriedt, "EBCM with multipole sources located in the complex plane," *Opt. Commun.* **139**, 85–98 (1997).
18. T. Wriedt and A. Doicu, "Formulations of the EBCM for three-dimensional scattering using the method of discrete sources," *J. Mod. Opt.* **45**, 199–213 (1998).
19. C. Müller, *Foundations of the Mathematical Theory of Electromagnetic Waves* (Springer-Verlag, New York, 1969).
20. V. V. Varadan, A. Lakhtakia, and V. K. Varadan, *Field Representation and Introduction to Scattering* (Elsevier, Amsterdam, 1991).